Land use and anthropogenic heat modulate ozone by meteorology: A perspective from the Yangtze River Delta region

Chenchao Zhan [a], Min Xie [a,*]

[a] School of Atmospheric Sciences, CMA-NJU Joint Laboratory for Climate Prediction Studies, Jiangsu Collaborative Innovation Center for Climate Change, Joint Center for Atmospheric Radar Research of CMA/NJU, Nanjing University, Nanjing 210023, China

----

[*] Corresponding author. minxie@nju.edu.cn (M. Xie)

Abstract: With the rapid advance in urbanization, land use and anthropogenic heat (AH) dictated by human activities significantly modify the urban climate and in turn the air quality. Focusing on the Yangtze River Delta (YRD) region, a highly urbanized coastal area with sever ozone (O_3) pollution, we estimate the impacts of land use and AH on meteorology and O_3 using the WRF-Chem model, which can enhance our understanding about the formation of O_3 pollution in those rapidly developing city clusters with place-specific topography as most of our results can be supported by previous studies conducted in other regions around the world. Regional O_3 pollution episodes occur frequently (~26 times per year) in the YRD in recent years. These O_3 pollution episodes are usually in calm conditions characterized by high temperature (over 20 °C), low relative humidity (less than 80%), light wind (less than 3 m s^{-1}) and shallow cloud cover (less than 5 okta). In this case, O_3 pollution belts tend to appear in the converging airflows associated with the sea and the lake breezes. The fast urbanization has significantly changed land use and AH in this region. The largest change in land use comes from the urban expansion, which causes an increase in 2-m temperature (T_2) by maximum 3 °C, an increase in planetary boundary layer height (PBLH) by maximum 500 m, a decrease in 10-m wind speed (WS_{10}) by maximum 1.5 m s^{-1} and an increase in surface O_3 by maximum 20 μg m^{-3}. With regard to the sea and lake breezes, the expansion of coastal cities, like Shanghai, can enhance the sea breeze circulation by ~1 m s^{-1}. During the advance of the sea breeze front inland, the updraft induced by the front makes well vertical mixing of O_3. However, once the sea breeze is fully-developed at afternoon (~17:00 LT), further progression inland will be stalled. Then the O_3 removal by the low sea breeze will be weakened and surface O_3 can be 10 μg m^{-3} higher

in the case with cities than no-cities. The expansion of lakeside cities, like Wuxi and Suzhou, can extend the lifetime of the lake breeze from noon to afternoon. Since the offshore flow of the lake breeze transports high O_3 from the land to the lake, the onshore flow brings the high O_3 back to the land. Surface O_3 in lakeside cities can increase as much as 30 μg m^{-3}. Compared to land use, the effects of AH are relatively small. And the changes mainly appear in and around cities where AH fluxes are large. There are increases in T_2, PBLH, WS_{10} and surface O_3 when AH are taken into account, with the increment of about 0.2 °C, 75 m, 0.3 m s^{-1} and 4 μg m^{-3}, respectively. AH contributes largely to the urban environment, altering meteorological factors, O_3 concentration and urban breeze circulation, but its effect on the sea and the lake breezes seems to be limited.

Key Words: ozone; local circulations; land use; anthropogenic heat; the Yangtze River Delta;

1 Introduction

Ozone (O_3) is a key constituent in the atmosphere, but acts quite differently in different parts of the atmosphere, often described as being "good up high and bad nearby". O_3 in the stratosphere helps protect life on earth from strong ultraviolet radiation. However, high O_3 in the troposphere is harmful to human respiratory system (Jerrett et al., 2009), the growth of vegetation (Mills et al., 2011) and climate (Worden et al., 2008). Therefore, tropospheric O_3 has long been regarded as an important air pollutant and has received continuous attention within the last few decades.

Tropospheric O_3 is mainly formed by a series of complex chemical reactions (Chameides and Walker, 1973; Xie et al., 2014) of precursor gases such as nitrogen oxides (NO_x=NO+NO_2) and volatile organic compounds (VOCs) in combination with sunlight. The global average lifetime of tropospheric O_3 is 20 to 25 days, and it will reduce to 5 days in boundary layer (Young et al., 2013). The relatively long lifetime of tropospheric O_3 favors regional/long-range transport, and brings huge challenges to its control (Bergin et al., 2005). O_3 levels considerably depend on the weather conditions because they play an important role in determining the chemistry, dispersion and removal of O_3 (Jacob and Winner, 2009). In general, elevated O_3 occurs under warm dry weather with strong sunlight, high temperature, low relative humidity and light wind speed (Zhang et al., 2015). Furthermore, weather conditions have many similarities in certain weather pattern (Buchholz et al., 2010; Zhan et al., 2019), and the main weather patterns associated with O_3 episodes in China are tropical cyclones and continental anticyclones (Wang et al., 2017).

O_3 concentrations as well as meteorology in urban areas are of great concern simply because urban areas have huge populations. A report from the United Nations pointed out that 69.6% of the world's population will live in cities by 2050. The urbanization process has also increased urban environmental hazards (Zhang et al., 2011), particularly in the most rapidly developing countries like China (Liu and Tian, 2010). Because of historical and cultural factors, many cities have similar topography, usually along the coast, close to mountains or in basins. For these cities, the local circulations induced by thermal contrast of the topography, such as sea-land breezes, mountain-valley breezes and lake-land breezes, have an important impact on urban air quality, especially under weak synoptic forcing (Crosman and Horel, 2010). Examples can be found around the world. Ding et al. (2004) simulated the main features of sea-land breezes during a multiday episode in the Pearl River Delta (PRD) region, and found that the sea-land breezes can transport air pollutants between inland and coastal cities. Miao et al. (2015) studied the effects of mountain-valley breezes on boundary layer structure in the Beijing-Tianjin-Hebei (BTH) region, suggesting that the mountain-valley breezes are vital to the vertical transport and distribution of air pollutants in Beijing. Wentworth et al. (2015) identified a causal link between lake breezes and O_3 in the Greater Toronto Area that the daytime O_3 maxima was 13.6-14.8 ppb higher on lake breeze days than no-lake breeze days.

Human activities, such as changes in land use and anthropogenic heat (AH), contribute to changes of meteorology and atmospheric compositions at local, regional and even global scales (Fu and Liao, 2014; Park et al., 2014; Oke et al., 2017). Land use changes via urban expansion (typically from vegetation to impervious surface) directly alters the surface physical properties (e.g., albedo, surface moisture and roughness), subsequently affecting the exchange of energy, moisture and momentum, and hence impacting the urban climate and air quality (Jiang et al., 2008; Wang et al., 2009). Li et al. (2019) found that increases in thermal inertia, surface roughness and evapotranspiration due to urban expansion can rise O_3 by 5.6 ppb in Southern California. AH is an important waste by-product of urban metabolism. Nearly all energy consumed by human activities will be dissipated as heat within Earth's land-atmosphere system (Flanner, 2009; Sailor, 2011) that is then "injected" into the energy balance processes. Ryu et al. (2013a) reported that AH affects the characteristics/structures of boundary layer and local circulations, resulting in an increase of O_3 by 3.8 ppb in the Seoul metropolitan area.

Previous studies usually investigated the impact of topography, land use and AH on meteorology and air quality separately, and mainly focusing on a specific megacity. However, these factors can work together in near-calm conditions. Furthermore, complex interactions exist widely among these thermally-driven circulations and the effects can even spread from one city to nearby areas. For example, Zhu et al. (2015) demonstrated that the meteorological conditions and air quality over Kunshan are significantly affected by Shanghai urban land surface forcing (Kunshan is located downstream of Shanghai, with a straight-line distance of about 50 km). Given the increasing prevalence of cities, cities gradually appear in the form of clusters. Therefore, assessing the effects of land use and AH (the topography rarely changes.) in the city cluster is meaningful, which helps understand the interactions between urban environment and human activities.

The Yangtze River Delta (YRD) region, located on the western coast of the Pacific Ocean (Figure 1a), has undergone accelerated urbanization process and rapid economic development over the past few decades. It is now one of the largest economic zones in the world. The YRD region consists of the southern part of Jiangsu Province, the northern part of Zhejiang Province and the eastern part of Anhui Province, including 26 mega/large cities such as Shanghai, Hangzhou and Nanjing (Figure 1b). With dense population and huge energy consumption, this area is now suffering from air quality deterioration (Xie et al., 2017; Zhan et al., 2020), especially the increasingly severe O_3 pollution in recent years (Li et al., 2020; Wang et al., 2020). Furthermore, cities with hot spots of O_3 usually concentrate in the central YRD region, surrounding Tai Lake (Zhan et al., 2021). Numerous cities, unique topography and sever O_3 pollution make the YRD an ideal study place.

In this study, the impacts of land use and AH on meteorology in the central YRD region, and how these impacts further modulate O_3 are investigated using the Weather Research and Forecasting model coupled to Chemistry (WRF-Chem). These results fill the knowledge gap about the formation of O_3 pollution in this region and provide valuable insight for other rapidly developing regions with complex topography in the world. The remainder of this paper is organized as follows. Sect. 2 gives a detailed description about the observation data, the model setup and experimental design. The main results, including the characteristics of O_3 pollution episodes, the model evaluation and the changes in meteorology and O_3 caused by land use and AH, are presented in Sect. 3. Summary and conclusions are given in Sect. 4.

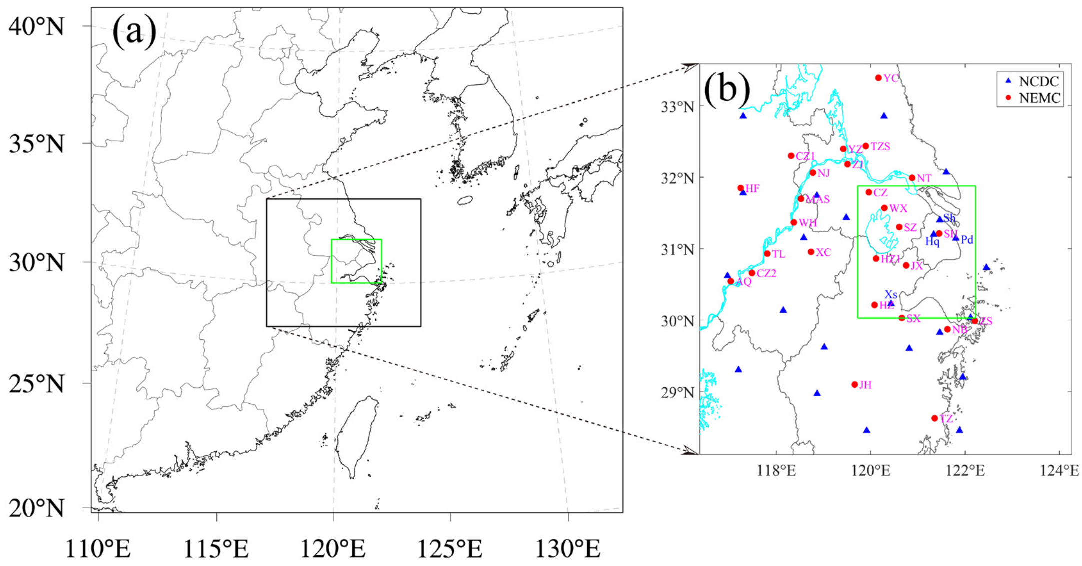

Figure 1. (a) Three nested WRF-Chem domains, (b) the locations of 26 cities (red dots) and weather stations (blue triangles) in the YRD. The green rectangular regions represent the innermost domain and also the central YRD region. These cities in (b) include: the megacity Shanghai (SH); Hangzhou (HZ), Ningbo (NB), Jiaxing (JX), Huzhou (HZ1), Shaoxing (SX), Jinhua (JH), Zhoushan (ZS) and Taizhou (TZ) located in Zhejiang Province; Nanjing (NJ), Wuxi (WX), Changzhou (CZ), Suzhou (SZ), Nantong (NT), Yancheng (YC), Yangzhou (YZ), Zhenjiang (ZJ) and Taizhoushi (TZS) located in Jiangsu Province; and Hefei (HF), Wuhu (WH), Maanshan (MAS), Tongling (TL), Anqing (AQ), Chuzhou (CZ1), Chizhou (CZ2) and Xuancheng (XC) located in Anhui Province.

2 Materials and methods

2.1 Surface observations

Hourly O_3 concentrations monitored by the National Environmental Monitoring Center (NEMC) of China are used in this study. These data strictly follow the national monitoring standards HJ 654-2013 and HJ 193-2013 (http://www.cnemc.cn/jcgf/dqhj/), and can be available at https://quotsoft.net/air/. The nationwide observation network initially operated in 74 major cities since 2013, and it has grown to more than 1,500 stations covering 454 cities by 2017 (Lu et al., 2018). The urban hourly O_3 concentrations are average results of measurements at all monitoring sites for each city. The maximum daily 8-h running average (MDA8) O_3 concentrations are then calculated based on the hourly O_3 concentration with more than 18-h measurements in the day (Liao et al., 2017).

Meteorological data are provided by the National Climatic Data Center (NCDC), including 2-m air temperature (T_2), relative humidity (RH), 10-m wind speed (WS_{10}) and direction (WD_{10}) and cloud cover (CC). These data as well as the technical documents recording the quality control, data collection and archive can be available at ftp://ftp.ncdc.noaa.gov/pub/data/noaa/isd-lite/. Locations of the surface observation stations are shown in Figure 1b. Specifically, the meteorological stations in the innermost domain include Pudong (Pd), Shanghai (Sh), Hongqiao (Hq) and Xiaoshan (Xs).

2.2 MODIS-based and USGS land use classifications

To explore the effects of land use on meteorology and O_3 in the YRD, two land use categories defaulted in WRF are used to set up the first two scenarios simulations (Table 2). The MODIS-based land cover product was created from 500-m MODIS Terra and Aqua satellite imagery (Friedl et al., 2010), and replaced USGS as the default settings in WRF since version 3.8. The USGS data primarily derived from the Advanced Very High Resolution Radiometer (AVHRR) from 1992 to 1993 at 1-km spatial resolution (Loveland et al., 2000), which reflects the distribution of cities in the late 1980s. Figure 2 presents the land cover maps in the innermost domain. The most obvious difference between MODIS and USGS comes from the urban fraction, which is related to the urban expansion caused by rapid urbanization in recent decades in the YRD. In addition, the Finer Resolution Observation and Monitoring-Global Land Cover in 2015 (GLC), which is one of the latest (2015) and finest (30-m) land cover datasets (Gong et al., 2019), is quite consistent with the performance of MODIS in this region. This confirms that urban fraction in MODIS is close to the reality. Thus, the MODIS data can generally refer to today's distribution of cities.

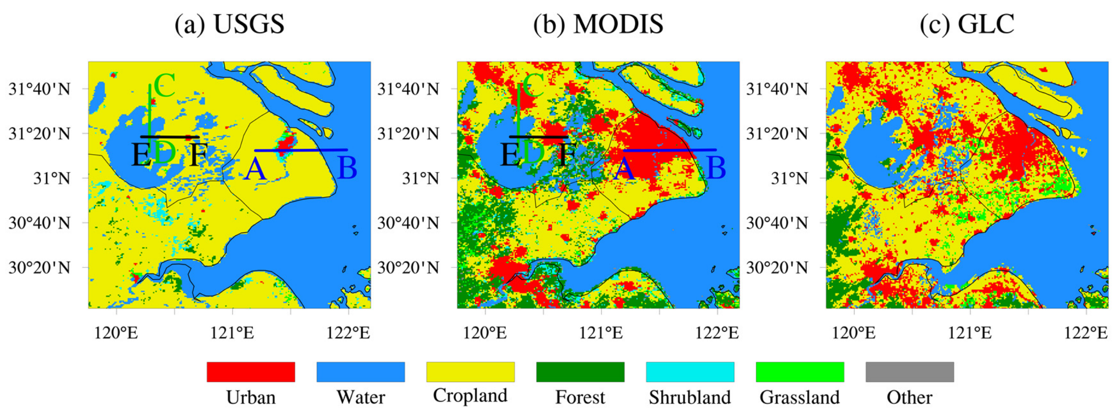

Figure 2. Land cover maps in the innermost domain, including the result of (a) USGS, (b) MODIS, and (c) GLC.

2.3 Anthropogenic heat flux modeling

Another scenario simulation incorporates the urban canopy model with the gridded AH fluxes to diagnose the impact of AH. The AH fluxes were calculated based on the statistics data of energy consumption of China in 2016, and then were grided as 144 rows and 144 columns with a resolution at 2.5° using population density downloaded from Columbia University's Socioeconomic Data and Applications Center. AH fluxes with their diurnal variations are considered by adding them to the sensible heat flux from the urban canopy layer within the Single Layer Urban Canopy Model (SLUCM). The AH fluxes for each grid are determined by the fixed AH value for the urban land use category, the urban fraction value on each grid and the fixed temporal diurnal pattern. Details on the calculation of AH fluxes, and how to add AH fluxes into the model can refer to Xie et al. (2016a, b). Figure 3 gives the spatial distribution of AH fluxes in the innermost domain. In the urban areas, the AH fluxes usually exceed 20 W m^{-2}. Some megacities, like Shanghai, can have a value of AH flux as high as 200 W m^{-2}. Except for the urban areas, the AH fluxes are generally less than 5 W m^{-2} in most parts of the YRD region. In particular, in those places where there is no human activity, the AH flux is 0.

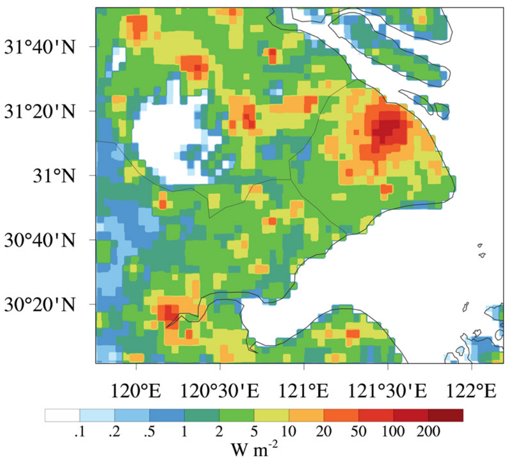

Figure 3. Spatial distribution of anthropogenic heat fluxes in the innermost domain.

2.4 Model setup and experimental designs

In this study, the WRF-Chem version 3.9.1 is applied. The WRF-Chem model is a fully coupled online numerical weather prediction model with chemistry component (Grell et al., 2005), in which chemical and the meteorological variables use the same coordinates, transport schemes and physics schemes in space and time. The initial and boundary conditions of meteorological fields are from the National Centers for Environmental Prediction (NCEP) global final analysis fields every 6 h with a spatial resolution of 1° × 1°. There are 32 vertical levels extending from the surface to 100 hPa with 12 levels located below 2 km to resolve the boundary layer processes. Furthermore, the domain and options for physical and chemical parameterization schemes are summarized in Table 1. The anthropogenic emissions are provided by the Multiresolution Emission Inventory for China (MEIC) in 2017 with a resolution of 0.25° (http://meicmodel.org/), which includes 10 air pollutants and CO_2 from power, industry, residential, transportation and agriculture sectors. The biogenic emissions are calculated online using the Model of Emissions of Gases and Aerosols from Nature (MEGAN) available in WRF-Chem (Guenther et al., 2006). As our main objective is to explore the response of O_3 to the meteorological changes induced by land use and AH, we use the same surface biogenic emission rates for different land use scenarios (Li et al., 2014, 2017). Further studies will be carried out to quantify the contribution of biogenic volatile organic compounds changed by meteorological conditions to O_3.

Table 1. The domains and major options for WRF-Chem

Items	Contents
Dimensions (x, y)	(101, 96), (146, 121), (236, 206)
Grid spacing (km)	25, 5, 1
Time step (s)	75
Microphysics	Purdue Lin microphysics scheme (Chen and Sun, 2002)
Longwave radiation	RRTM scheme (Mlawer et al., 1997)
Shortwave radiation	Goddard scheme (Kim and Wang, 2011)
Surface layer	Revised MM5 Monin-Obukhov scheme
Land-surface layer	Noah land-surface model (Chen and Dudhia, 2001)
Planetary boundary layer	YSU scheme (Hong et al., 2006)

Cumulus parameterization	Grell 3D ensemble scheme (Grell and Devenyi, 2002)
Gas-phase chemistry	RADM2 (Stockwelll et al., 1990)
Photolysis scheme	Fast-J photolysis (Fast et al., 2006)
Aerosol module	MADE/SORGAM (Schell et al., 2001)

As shown in Table 2, three numerical experiments are performed. The MODIS_noAH experiment is a control simulation with commonly used settings. Compared with MODIS_noAH, USGS_noAH selects the USGS land use classification at run-time through the geogrid program. Thus, the difference between the modeling results of MODIS_noAH and USGS_noAH can illustrate the changes caused by land use. As for the impact of AH, it can be identified by comparing the modeling results of MODIS_AH and MODIS_noAH. To exclude the uncertainty conceivably caused by different configurations, all three simulations use the same emission inventory, physical and chemical parameterization schemes (Table 1), running from 00:00 UTC 21 May to 00:00 UTC 4 June 2017 with the first 88 h as spin-up time.

Table 2. The three numerical experiments.

Scenario	Land use classification	Whether to add AH
MODIS_noAH	MODIS-based	No
USGS_noAH	USGS	No
MODIS_AH	MODIS-based	Yes

2.5 Model evaluation

To verify model performance, the simulation results in the innermost domain, including O_3 concentration, T_2, RH, WS_{10} and WD_{10} are examined against the surface observations described in Sect. 2.1. The statistical metrics, including the mean bias (MB), root mean square error (RMSE) and correlation coefficient (COR), are also calculated. They are defined as follows:

$$MB = \frac{1}{N}\sum_{i=1}^{N}(\mathrm{S}_i - \mathrm{O}_i), \tag{1}$$

$$RMSE = \sqrt{\frac{1}{N}\sum_{i=1}^{N}(\mathrm{S}_i - \mathrm{O}_i)^2}, \tag{2}$$

$$COR = \frac{\sum_{i=1}^{N}(\mathrm{S}_i - \overline{\mathrm{S}})(\mathrm{O}_i - \overline{\mathrm{O}})}{\sqrt{\sum_{i=1}^{N}(\mathrm{S}_i - \overline{\mathrm{S}})^2}\sqrt{\sum_{i=1}^{N}(\mathrm{O}_i - \overline{\mathrm{O}})^2}}, \tag{3}$$

where S_i and O_i are the simulations and observations, respectively. *N* is the total amount of valid data, and $\overline{\mathrm{S}}$ and $\overline{\mathrm{O}}$ represent the average of simulations and observations, respectively. Generally, the model performance is acceptable if the values of *MB* and *RMSE* are close to 0, and that of *COR* is close to 1 (Xie et al., 2016a, b; Zhan et al., 2020).

3 Results and discussions

3.1 Regional O_3 pollution episodes in the YRD

On cloudless sunny days, regional O_3 pollution episodes occur frequently in the YRD (Gao et al., 2020; Zhan et al., 2021), which can affect an area of up to 3.5 million square kilometers and harm more than 200 million people. The regional O_3 pollution is generally defined as when more than half of the 26 typical cities in the YRD fail to meet the national O_3 standard (In China, the national ambient air quality standard for MDA8 O_3 is 160 μg m^{-3}). Based on the surface O_3 observations, we sort out all regional O_3 pollution episodes and the corresponding weather patterns from 2015 to 2019 (Table S1). There were 20, 19, 34, 28 and 30 regional O_3 pollution cases in the YRD from 2015 to 2019, respectively. These cases mainly occurred in April to October of each year, and were usually related to high pressure, uniform pressure field and typhoon activity.

Figure 4 further displays the monthly distribution of meteorological factors during the day (from 8:00 to 20:00 local time) when regional O_3 pollution occurs in the YRD. All the variables show significant monthly variations. The highest (lowest) temperature is found in July (April), and the relative humidity is highest in June. As for the cloud cover, the sky is covered with fewer clouds in October than other months. In addition, southeast wind prevails in the YRD from April to October under the influence of monsoon climate. The correlation coefficients between temperature, relative humidity, cloud cover, wind speed and MDA8 O_3 are 0.12, -0.34, -0.15 and 0.04, respectively. O_3 pollution episodes tend to occur on days characterized by high temperature, low relative humidity, cloudless sky and light wind (the weak correlation between wind speed and MDA8 O_3 is due to the small change in light wind). More specifically, on days when the temperature exceeds 20 ℃ (Figure 4b), the relative humidity is less than 80% (Figure 4c), the cloud cover is less than 5 okta (Figure 4d), and the wind speed is less than 3 m s^{-1} (Figure 4e) in the YRD. On the other hand, local circulations are clearest when in absence of clouds, radiative heating is strongest and wind is weakest. In this case, local circulation can inevitably have an impact on the evolution of O_3.

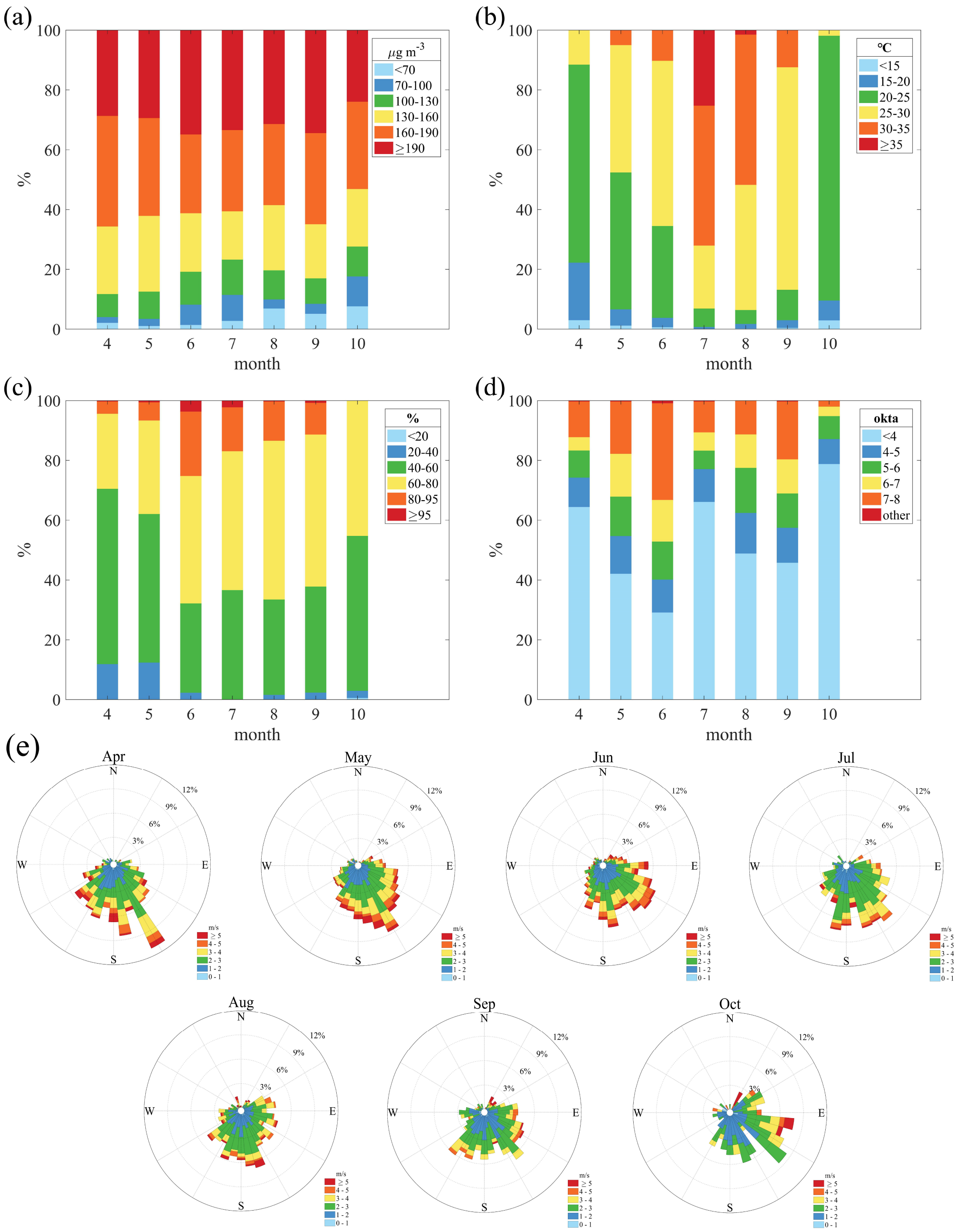

Figure 4. The monthly distribution of (a) MDA8 O_3, (b) temperature, (c) relative humidity, (d) cloud cover, and (e) wind speed and direction during the daytime (8:00 to 20:00 LT) when regional O_3 pollution occurs in the YRD.

3.2 Case selection

3.2.1 Case for O_3 pollution episode

For simplicity but without loss of generality, the longest-lasting regional O_3 pollution episode is selected to investigate the impacts of land use and AH on meteorology and O_3 in the YRD. This 10-day regional O_3 pollution episode occurred from 25 May to 3 June in 2017 (Table S1). Dominated by high pressure/uniform pressure field (Figure S1), high O_3 concentrations are accompanied by high air temperature, low relative humidity, light wind and shallow cloud cover during this smog episode. An average of 18 out of the 26 cities experienced O_3 pollution every day with MDA8 O_3 concentrations ranged from 80.0 to 269.0 μg m^{-3} in the YRD. With regard to the meteorological factors, T_2 ranged from 12.9 to 33.5 °C, with an average of 26.4 °C; RH ranged from 26.6 to 99.4 %, with an average of 58.6 %; WS_{10} ranged from 0.5 to 10.8 m s^{-1}, with an average of 2.8 m s^{-1}; CC ranged from 0 to 8.4 okta, with an average of 4.2 okta (Table 3). The values of these meteorological factors meet the standards in previous section, and can cover both the whole YRD and the central YRD region (the innermost domain). Therefore, this O_3 pollution episode not only meets the requirements of high O_3 concentration but also clam weather conditions. And the long duration provides relatively universal results.

Table 3. Mean, minimum and maximum of MDA8 O_3, T_2, RH, WS_{10} and CC during the daytime from 25 May to 3 June 2017.

	The YRD region			The central YRD region		
	Mean	Minimum	Maximum	Mean	Minimum	Maximum
MDA8 O_3 (μg m^{-3})	182.1	80.0	269.0	177.8	118.0	251.0
T_2 (°C)	26.4	12.9	33.5	26.7	21.4	29.8
RH (%)	58.6	26.6	99.4	52.9	33.8	73.7
WS_{10} (m s^{-1})	2.8	0.5	10.8	3.6	1.6	6.0
CC (okta)	4.2	0	8.4	3.3	0	7.4

3.2.2 Evaluation of model performance

To evaluate the model performance, the simulation results in the innermost domain are validated by comparing with the observational data. Table 4 presents the statistical metrics in meteorological factors. Figure 5 further illustrates the time series of these meteorological factors and their modeling results. T_2 is reasonably well simulated as the CORs (the mean of all the sites) are 0.87, 0.86 and 0.86 in MODIS_noAH, USGS_noAH and MODIS_AH, respectively. The small negative MBs at all sites suggest that our simulations underestimate T_2 to some extent, though this light underestimation is acceptable because of the small RMSEs (2.3, 3.1 and 2.3 ℃). The MBs for T_2 in USGS_noAH, MODIS_noAH and MODIS_AH are -2.4, -1.0, and -0.8 ℃, indicting an improvement in temperature when new land use and AH are taken into account. This can also be confirmed by Figure 5a. With respect to RH, the CORs are 0.82, 0.75 and 0.83 for MODIS_noAH, USGS_noAH and MODIS_AH, respectively. Thus, all three simulations can well capture the diurnal variation of RH, but have different performance on different sites (Figure 5b). In USGS_noAH, RH is overestimated at all sites, especially Pudong site with the MB is 11.2%. While RH is overestimated at the two coastal sites (Pudong and Shanghai) but underestimated at other two sites (Hongqiao and Xiaoshan) in MODIS_noAH and MODIS_AH. Moreover, USGS_noAH has the highest RMSEs of RH (16.3%), followed by MODIS_AH (12.4%) and MODIS_noAH (12.1%). As for WS_{10}, the modeling values are slightly overestimated at all sites in all three simulations. The overestimation of WS_{10} may partly be attributed to the unresolved terrain features by the default surface drag parameterization causing an overestimation of wind speed especially at low values (Jimenez and Dudhia, 2012). In particular, WS_{10} in USGS_noAH is the most overestimated, followed by MODIS_AH and MODIS_noAH with the MBs are 1.2, 1.0 and 0.8 m s^{-1}, respectively. In addition, high MBs of WS_{10} are corresponding to high RMSEs (1.9, 1.8 and 1.7 m s^{-1}) in our simulations. In terms of WD_{10}, the model captures well the shift in wind direction during the study period (Figure 5d). Thus, our modeling results of wind speed and direction basically reflect the characteristics of wind fields. In summary, both the statistical metrics in Table 4 and time series in Figure 5 indicate that all three numerical experiments can capture the major changes about meteorological factors during this O_3 pollution episode. Nevertheless, updating the land use and adding AH can somewhat reduce the underestimation of T_2 and the overestimation of RH and WS_{10} in models.

Table 4. Statistical metrics in meteorological variables between observations and simulations.

Variables	Site		MODIS_noAH				USGS_noAH				MODIS_AH			
		$\bar{O}$[a]	$\bar{S}$[b]	MB[c]	RMSE[d]	COR[e]	$\bar{S}$	MB	RMSE	COR	$\bar{S}$	MB	RMSE	COR
T_2	Pd	23.2	21.5	-1.7	2.4	0.89	20.7	-2.5	3.8	0.70	21.5	-1.7	2.4	0.89
(°C)	Sh	24.6	23.9	-0.7	2.2	0.87	22.5	-2.1	2.7	0.90	24.2	-0.5	2.3	0.84
	Hq	25.3	24.4	-0.9	2.0	0.89	22.7	-2.6	3.0	0.95	24.8	-0.5	1.9	0.89
	Xs	25.9	25.1	-0.8	2.4	0.85	23.8	-2.2	2.8	0.91	25.5	-0.4	2.4	0.83
RH	Pd	69.1	77.7	8.6	13.5	0.81	86.2	17.2	23.4	0.45	77.7	8.7	13.3	0.83
(%)	Sh	59.3	60.6	1.3	11.7	0.81	71.1	11.8	16.1	0.81	59.4	0.1	12.4	0.78
	Hq	59.5	57.7	-1.8	9.8	0.88	70.6	11.1	14.5	0.89	56.2	-3.3	9.8	0.89
	Xs	60.6	55.4	-5.2	13.5	0.79	65.3	4.8	11.3	0.86	53.5	-7.1	14.1	0.80
WS_{10}	Pd	4.1	4.1	0.0	1.4	0.47	5.5	1.3	2.1	0.35	4.2	0.1	1.3	0.51
($m\ s^{-1}$)	Sh	2.5	4.2	1.7	2.2	0.36	4.5	2.0	2.4	0.54	4.3	1.9	2.3	0.35
	Hq	3.7	3.9	0.2	1.2	0.54	3.9	0.2	1.2	0.53	4.2	0.5	1.3	0.50
	Xs	2.3	3.6	1.3	2.0	0.26	3.4	1.1	1.8	0.30	3.8	1.5	2.1	0.24
WD_{10}	Pd	160.4	136.1	-26.2	78.7	0.42	148.1	-14.3	55.1	0.72	137.3	-24.7	77.5	0.42
(°)	Sh	141.6	146.4	4.8	66.4	0.60	141.7	0.1	63.9	0.59	142.6	1.0	69.9	0.56
	Hq	159.7	140.2	-23.4	80.2	0.46	153.1	-10.6	74.9	0.52	142.8	-20.4	91.8	0.29
	Xs	188.6	160.2	-28.4	99.5	0.48	161.4	-27.3	109.6	0.35	152.0	-36.6	109.9	0.38

[a] $\bar{O}$ and [b] $\bar{S}$ indicate the average of observations and simulations, respectively. [c] MB indicates the mean bias, [d] RMSE indicates the root mean square error and [e] COR indicate the correlation coefficient, with statistically significant at 99% confident level.

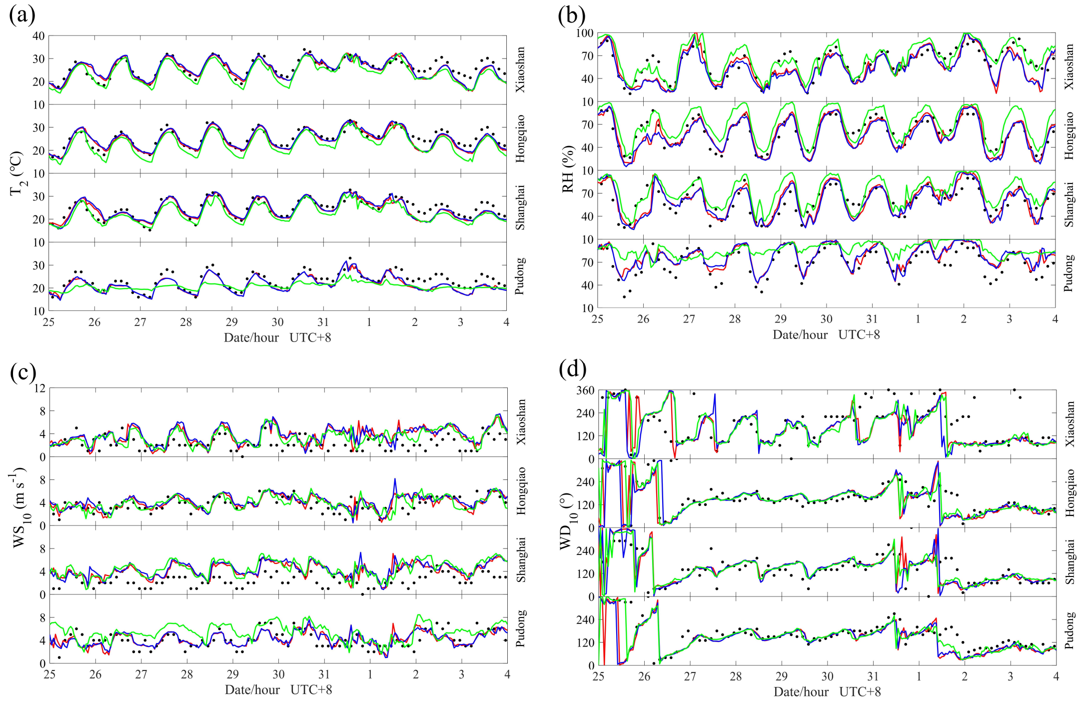

Figure 5. Time series of T_2, RH, WS_{10} and WD_{10} for observations and simulations at different weather stations. The black dots are the surface observations. The simulation results of MODIS_noAH, USGS_noAH and MODIS_AH are shown in red, green and blue lines, respectively.

Table 5 lists the statistical metrics in O_3, and Figure 6 gives the hourly variations of O_3 for observations and simulations in different cities. With high CORs (the CORs are 0.80, 0.81 and 0.80 in MODIS_noAH, USGS_noAH and MODIS_AH, respectively), all three simulations well reproduce the diurnal variation of O_3, which is that O_3 concentration reaches its maximum in the afternoon and gradually decreases to its minimum in the morning. The magnitudes of O_3 modeling results are reasonable (Figure 6), but the peak and valley values of O_3 simulations are sometimes differ from the observations, especially the peak value, like Huzhou. Considering the relatively low MBs (6.9, -1.6 and 9.0 μg m^{-3}) and RMSEs (49.3, 46.2 and 49.0 μg m^{-3}), the modeling results of O_3 are generally reasonable and acceptable.

Table 5. Statistical metrics in O_3 (μg m^{-3}) between observations and simulations.

Case	Index	City						
		CZ	WX	SZ	SH	HZ1	JX	HZ

	$\overline{O}$	89.7	141.8	121.7	112.8	95.8	113.2	104.8
MODIS_noAH	$\overline{S}$	123.2	117.6	116.2	103.4	128.1	112.5	127.5
	MB	33.3	-24.2	-5.6	-9.1	32.1	-0.6	22.7
	RMSE	53.8	49.1	42.8	36.4	59.9	44.4	58.6
	COR	0.85	0.83	0.82	0.80	0.83	0.78	0.71
USGS_noAH	$\overline{S}$	108.1	106.8	107.1	93.8	118.6	111.0	122.5
	MB	18.5	-35.0	-14.7	-18.9	23.0	-2.0	18.0
	RMSE	43.5	56.0	44.7	37.7	50.1	41.1	50.0
	COR	0.83	0.81	0.80	0.81	0.82	0.80	0.77
MODIS_AH	$\overline{S}$	124.5	119.8	119.1	108.0	130.3	113.7	127.8
	MB	34.7	-21.9	-2.7	-4.6	34.3	0.6	23.0
	RMSE	53.5	47.3	42.4	37.4	59.4	44.7	58.2
	COR	0.84	0.83	0.81	0.80	0.82	0.78	0.71

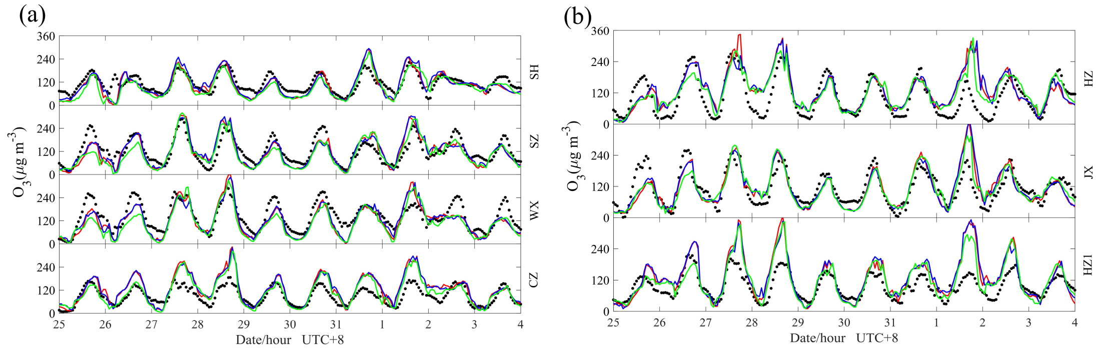

Figure 6. Same as Figure 5, but for O_3.

Above all, the WRF-Chem model using our configuration has a good capability in simulating the meteorological factors and O_3 over the studied region. In addition, it is noteworthy that the object of inter-comparisons between the three numerical experiments are not to determine which setting is the most skillful in reproducing the observations. Rather, it is to diagnose and understand the changes induced by land use and AH, and the response of O_3 to these changes.

3.3 Overall behaviors of O_3 and local circulations

Based on the results of the control simulation (MODIS_noAH), we first give an overall behavior of O_3 and local circulations during the study period. Then the changes induced by land use and AH are discussed via inter-comparisons between different scenarios simulations. Thereby, only difference plots between USGS_noAH/MODIS_AH and MODIS_noAH are shown in this paper, and the corresponding original plots for USGS_noAH/MODIS_AH can be found in the supplementary materials (Figure S2-7).

3.3.1 Spatiotemporal variations of O_3

As show in Figure 7, O_3 concentration began to rise around 8:00 local time (LT = UTC + 8 h), and became noticeable after only 3 hours (Figure 7a and h). During this stage, the nocturnal residual layer vanished due to the development of the convective boundary layer (Figure 8). The O_3-rich air mass in the residual layer was mixed with the O_3-poor air mass on the ground, which enhanced the surface O_3 in the morning (Hu et al., 2018). Around 11:00 LT, the convective boundary layer was established (Figure 8), and high O_3 produced by photochemical reactions appeared over the central YRD and persisted until 18:00 LT (Figure 7b and c). After sunset, surface O_3 concentration generally decreased due to nitrogen oxide (NO) titration, and reached its minimum in the early morning (Figure 7f and g). In general, O_3 has a typical diurnal variation with high concentration in the daytime and low concentration at night. This is consistent with the observations in Figure 6, and this rule of O_3 can be applied to most parts of the world. Therefore, the situation during the daytime (we select 11:00, 14:00, 17:00 and 20:00 LT in this study) should be paid attention to when it comes to O_3 pollution.

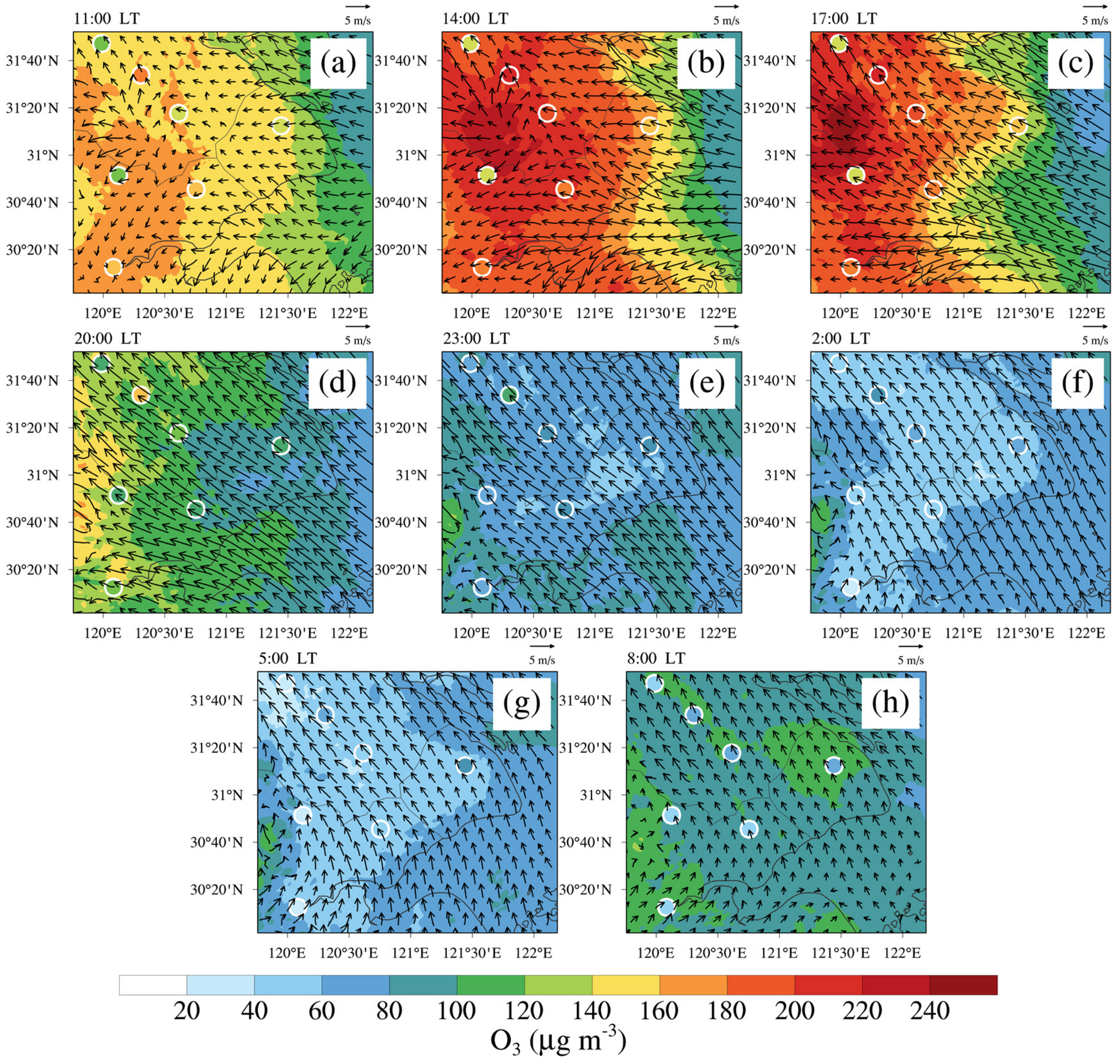

Figure 7. Horizontal distributions of O_3 and wind at the lowest model level in MODIS_noAH. (a), (b), (c) and (d) are the results at 11:00, 14:00, 17:00 and 20:00 LT, referring to the daytime. (e), (f), (g) and (h) are the results at 23:00, 2:00, 5:00 and 8:00 LT, referring to the night. The observations in different cities are overlaid using colored circles. To obtain universal feature, all results are the average of the study period, and the same for the subsequent results.

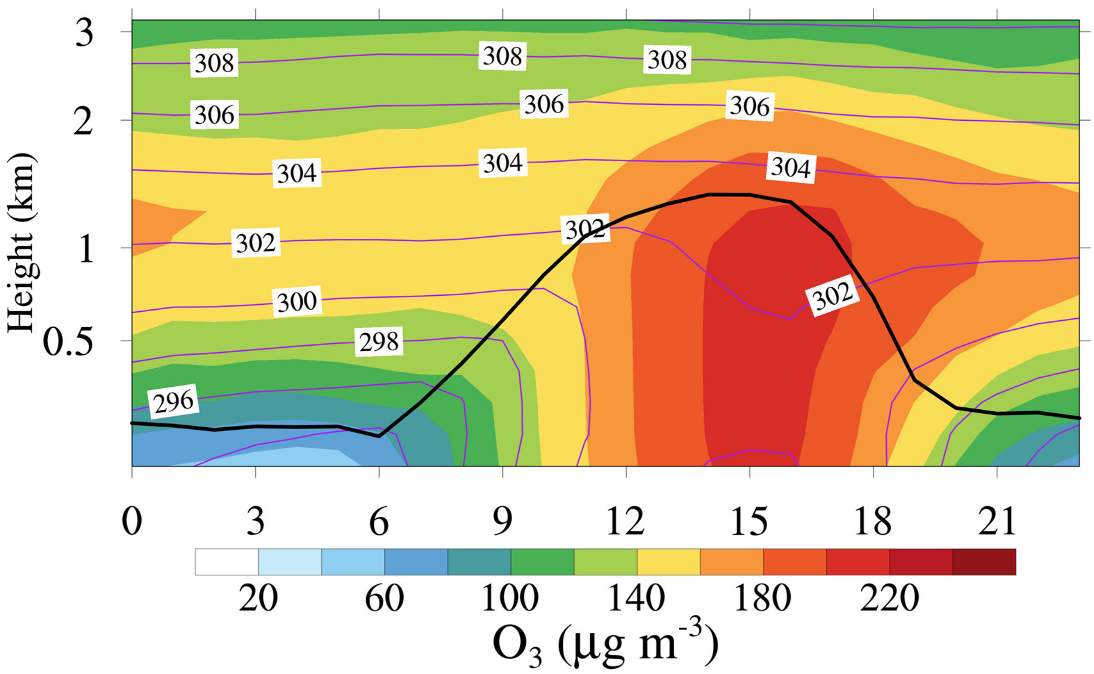

Figure 8. Temporal-vertical distribution of O_3 and potential temperature covering the CZ, WX, SZ, SH, HZ1, JX and HZ over the innermost domain of MODIS_noAH.

3.3.2 Sea and lake breezes

As shown in Figure 7a and b, high O_3 concentration in the central YRD tended to appear in the converging airflows associated with the sea breeze, the lake breeze and background southeast wind (Figure 4e). The sea breeze and the background southeast wind were usually in the same direction, and thereby sea breeze affected a wide area and lasted a long time. The sea breeze was obvious around 14:00 LT and matured around 17:00 LT, and continuously transported high O_3 from coastal to inland areas during this period (Figure 7b-d). Compared with the sea breeze, the lake breeze had a much smaller influencing area and a shorter duration. Around 11:00 LT, the lake breeze was established. It reached its maximum intensity around 14:00 LT, and then disappeared sharply due to the predominant southeast wind (Figure 7b and c). Both the sea and the lake breezes are the typical local circulations in the YRD, which plays important roles in the horizontal distributions of O_3 over this region.

Since the coastline is generally north-south (Figure 1b), the cross sections along blue line AB depicted in Figure 2a are illustrated to show representative example of the vertical structure of the sea breeze (Figure 9a-c). By 11:00 LT, the sea breeze below 500m had already developed. The sea breeze front was found in front of Shanghai (~121.6°E), with a height of 1.5 km. Around 14:00 LT, the speed of sea breeze increased, which exceeded 5 m s^{-1}. The sea breeze front moved inland for a distance of 20-30 km (~121.4°E), and was elevated to ~2 km (Figure 9b). Around 17:00 LT, strong sea breeze swept across the central YRD, reducing the O_3 concentration near the surface in Shanghai. But the O_3 in the mixed layer still maintained a high level, which may result in an O_3-rich reservoir forming in the nocturnal residual layer (Figure 9c). The penetration of sea breeze front and its effect on surface O_3 are also observed in other coastal regions, such as Taiwan (Lin et al., 2007), the Athens basin (Mavrakou et al., 2012) and Paulo (Freitas et al., 2007).

As for the lake breeze, the cross sections along green line CD and black line EF in Figure 2a are given since the lake is usually inside the land so that the lake breeze can have different directions. The lake breeze was established by 11:00 LT (Figure 9d and g) though it was shallow at that time. Around 14:00 LT, the lake breeze strengthened. The extension of the lake breeze circulation zone can even reach up to 2 km in the vertical dimension (Figure 9e). The offshore flow of the lake breeze circulation (~2 m s^{-1}) transported high O_3 concentration from the urban areas to the lake, while the onshore flow blew the O_3 back to urban areas (Figure 9e and h). Thus, the net effect of the lake breeze is to accelerate the vertical mixing of O_3 in the boundary layer, resulting in high surface O_3 in the lakeside cities. This was also reported in other lakeside cities, such as the Lake Michigan (Lennartson and Schwartz, 2002), the Great Lakes (Sills et al., 2011) and the Great Salt Lake (Blaylock et al., 2017). By 17:00 LT, the lake breeze disappeared.

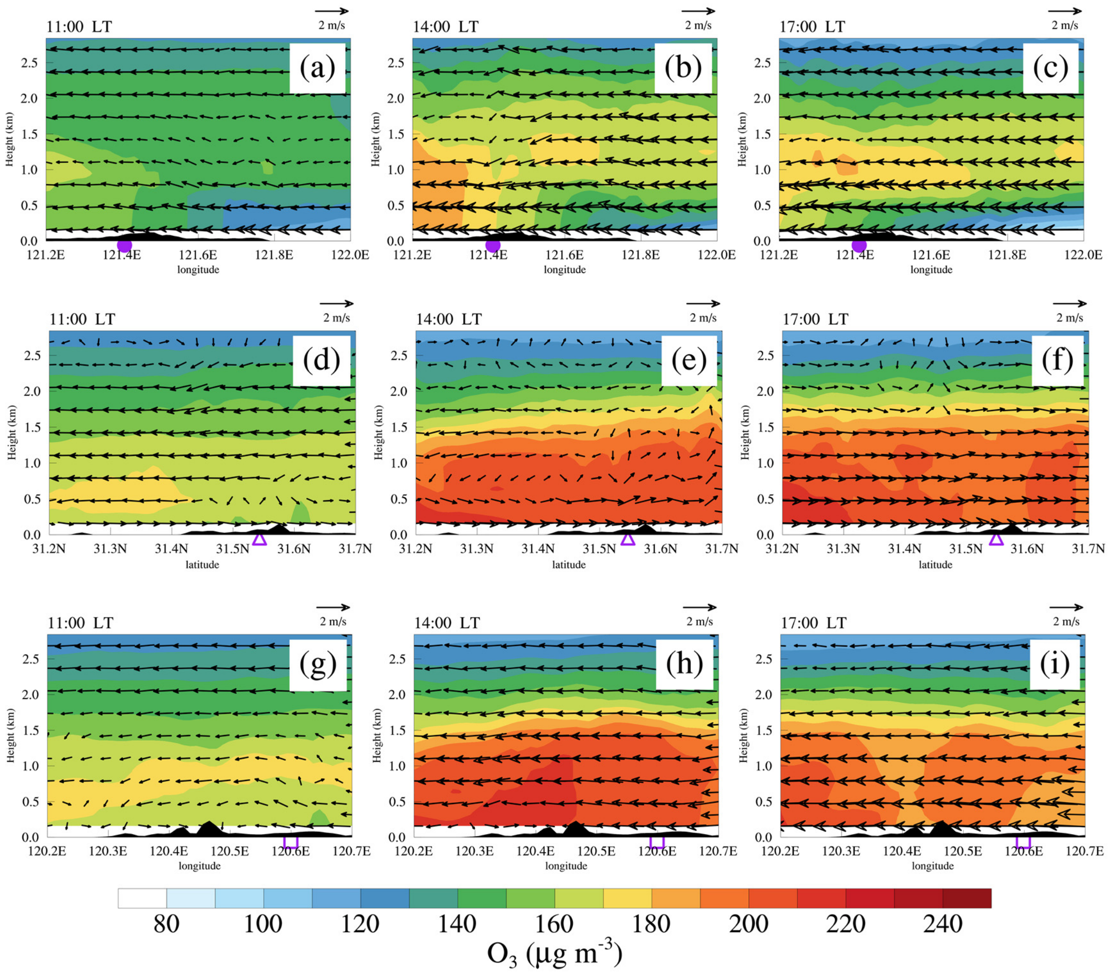

Figure 9. Vertical cross sections of O_3 and wind for the sea breeze at (a) 11:00, (b) 14:00 and (c) 17:00 LT along blue line AB in Figure 2a. (d), (e) and (f) are the same as (a), (b) and (c), respectively, but for the lake breeze along green line CD in Figure 2a. (g), (h) and (i) are also the same as (a), (b) and (c), respectively, but for the lake breeze along black line EF in Figure 2a. The purple dots, triangles and rectangles represent the locations of Shanghai, Wuxi and Suzhou, respectively. The black shaded areas represent the terrain, and the terrain has been multiplied by a factor of 10 when plotting.

3.4 Impacts of land use on meteorology and O_3

3.4.1 The changes in horizontal direction

Figure 10 presents the spatial differences of the main factors (T_2, PBLH, WS_{10} and O_3) between MODIS_noAH and USGS_noAH. Land use changes via urban expansion can enhance surface heating through upward sensible heat fluxes so that T_2 will increase. As shown in Figure 10a-d, the spatial pattern of remarkable warming effect for T_2 was consistent with the urban-fraction change associated with the urbanization (Figure 2a and b), which is the positive temperature anomaly mainly appeared in cities and their surrounding areas. In megacities like Shanghai, T_2 increased by even 3 ℃. The change in PBLH was similar to that in T_2 because the warming up of T_2 was conductive to the vertical movement in the boundary layer, which increased the PBLH (Figure 10e-h). The maximum positive change of PBLH can reach up to 500 m at noon but down to 100 m after sunset. With regard to the WS_{10}, it decreased in the MODIS_noAH (Figure 10i-l), with a maximum decrease up to 1.5 m s^{-1} in Hangzhou around 17:00 LT. This is because the roughness of cities and forest is larger than that of cropland (Figure 2a and b). Apart from the abovementioned meteorological factors, urban expansion also increased the surface O_3 concentration (Figure 10m-p). The largest increment of O_3 appeared in the afternoon, with a value of 20 μg m^{-3} around 17:00 LT in Changzhou. In addition to these results, it is noteworthy that there were confusing "false" changes at the junction of land and sea/lake, especially for meteorological factors, such as T_2 and WS_{10}. This was caused by the different treatment of the MODIS-based and USGS land use classifications at the boundary conditions of land versus water instead of urban expansion.

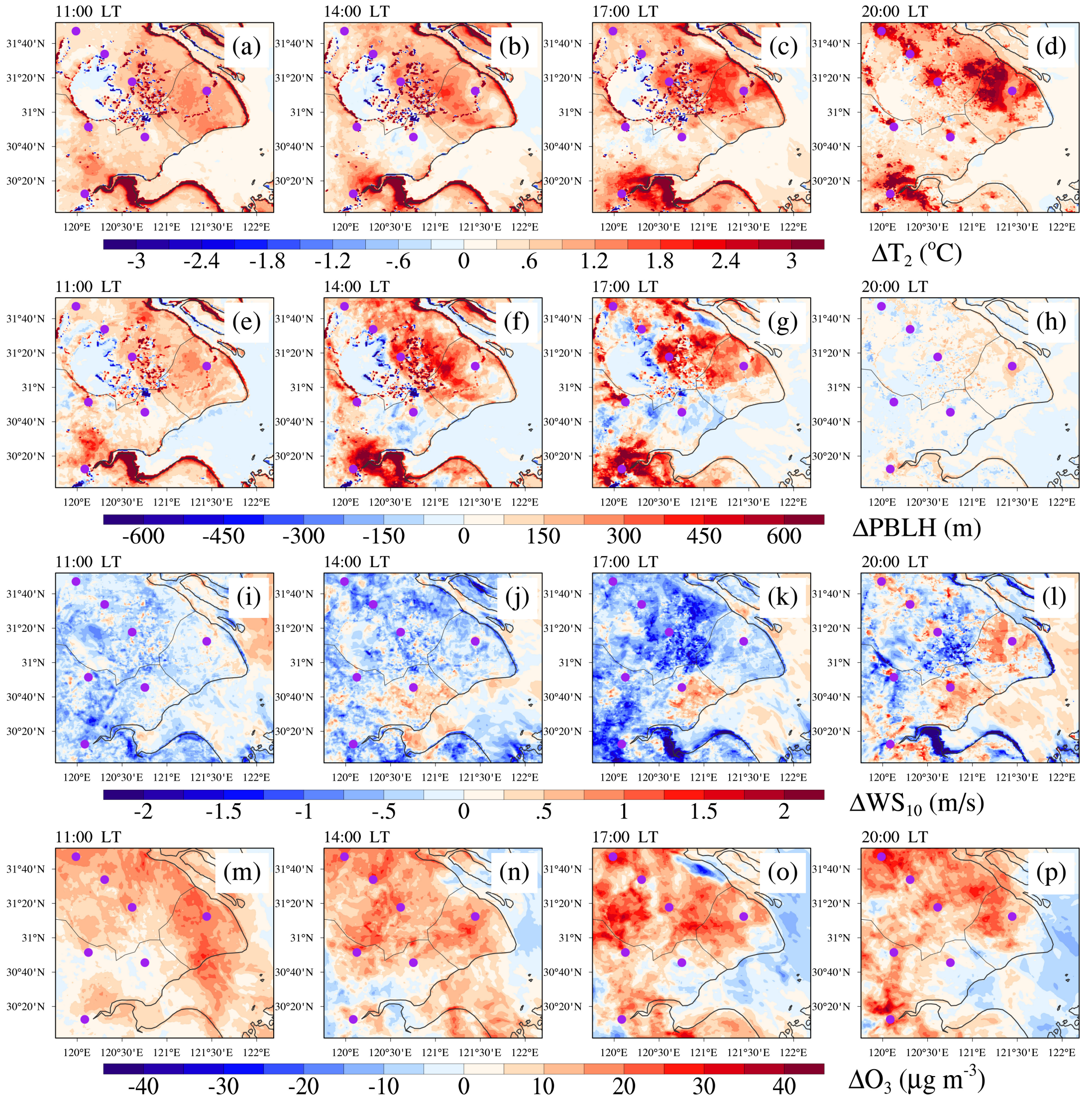

Figure 10. Horizontal distributions of the differences of (a-d) T_2, (e-h) PBLH, (i-l) WS_{10} and (m-p) O_3 differences between MODIS_noAH and USGS_noAH (MODIS_noAH – USGS_noAH) during the daytime. The purple dots represent the locations of cities in the innermost domain.

3.4.2 The changes in vertical direction

Urban expansion not only alters the meteorological factors, but also the local circulations. As shown in Figure 11a-c, the sea breeze below 500 m increased by ~1 m s^{-1} due to the enhanced temperature contrast between the land and the sea induced by the expansion of Shanghai. During the advance of the sea breeze front inland, the updraft induced by the sea breeze front promoted the vertical mixing of O_3, elevating surface O_3 concentration in Shanghai (Figure 11a and b). When the sea breeze matured around 17:00 LT, its transport effect reduced the surface O_3 concentration of the coastal cities (Figure 9c). However, this "transport effect" was weakened because the sea breeze near the surface was slowed affected by the rough urban surface. Finally, surface O_3 of ~10 μg m^{-3} was left compared to the scenario without cities. In contrast to the onshore flow, the offshore flow transported high concentration of O_3 to the sea, which may be an important source of O_3 in the nocturnal residual layer. Influenced by the strong background southeast wind, the offshore flow was imperceptible during the day (Figure 9), but it can be enhanced by urban expansion (Figure 11c).

As for the lake breeze, it was also enhanced by ~1 m s^{-1} because of the larger temperature contrast resulting from expansion of lakeside cities (Figure 11e and h).What's more, the life of the lake breeze was extended to 17:00 LT (Figure 11f and i). Since the lake breeze circulation was conducive to the vertical mixing in the boundary layer, and its onshore flow transported high concentration of O_3 from the lake to the city (Sect. 3.3.2), the O_3 concentration will increase in the lakeside cities, with a maximum of 30 μg m^{-3} in Wuxi at 14:00 LT.

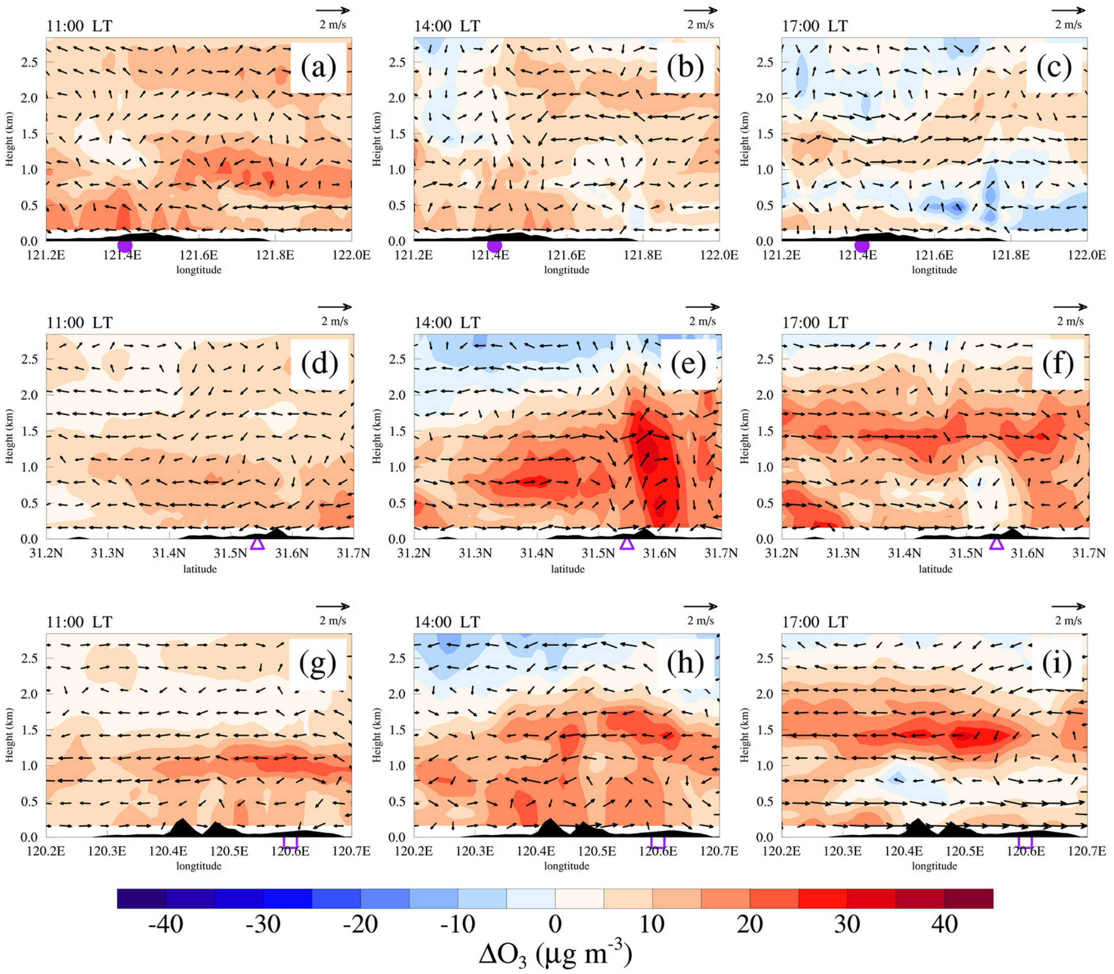

Figure 11. Same as Figure 9, but for the differences between MODIS_noAH and USGS_noAH (MODIS_noAH – USGS_noAH).

3.4.3 The mechanism of land use modulating O_3

Changing land use from USGS to MODIS leads to an increase in T_2 by maximum 3 ℃, an increase in PBLH by maximum 500 m and a decrease in WS_{10} by maximum 1.5 m s^{-1} in the YRD, which is comparable to those in the BTH region (Yu et al., 2012), the PRD region (Li et al., 2014) and the National Capital Region of India (Sati and Mohan, 2017). These changes are particularly evident in and around cities as the biggest change in land use is related to urban expansion. The elevated air temperature is conducive to the photochemical production of O_3, and the well-developed boundary layer favors the vertical mixing of O_3. These changes in meteorological factors eventually increase the surface O_3 concentration by maximum 20 μg m^{-3} in the YRD. Furthermore, local circulations, including the sea and lake breeze, are also influenced by urban expansion, which further alters O_3 in the vertical direction. For the coastal cities, like Shanghai, the larger temperature contrast caused by cities enhances the sea breeze below 500 m. As the sea breeze front moves inland, it enhances upward movement, which is conductive to the mixing of O_3 in the boundary layer. However, the movement of the sea breeze is slowed due to the rough urban surface after the sea breeze matures. The removal of the sea breeze near the surface is then weakened. The similar response of the sea breeze to cities as well as its impact on O_3 has been also reported in the PRD region (You et al., 2019) and Paulo (Freitas et al., 2007). For the lakeside cities, like Wuxi and Suzhou, the lifetime of the lake breeze is extended to the afternoon due to the expansion of cities. The offshore flow of the lake breeze transports high O_3 concentration in the middle of the boundary layer from the land to the lake, while the onshore flow brings the O_3 back to the land, which accelerates the vertical mixing of O_3 and increases the surface O_3. Thus, high surface O_3 usually appears when the lake breeze is established. This was also observed in the Greater Toronto Area (Wentworth et al., 2015) and the Lake Michigan (Abdi-Oskouei et al., 2020).

3.5 Impacts of anthropogenic heat on meteorology and O_3

3.5.1 Horizontal changes

Compared with land use, the changes caused by AH are much smaller (Figure 12). Furthermore, these changes are effective in and around cities as they usually have large AH flux density (Figure 3). By adding more surface sensible heat into the atmosphere, the AH fluxes leaded to an increase in T_2 of 0.2 ℃ in urban areas, with the typical value of 0.42 ℃ in Shanghai (Figure 12a-d). Vertical air movement in the boundary layer was then enhanced by the warming of T_2, and the PBLH will increase as well. According to the simulations, the PBLH increased by ~75 m in the urban areas (Figure 12e-h). Contrary to the decrease in WS_{10} caused by urban expansion, WS_{10} increased by ~0.3 m s^{-1} in the urban areas when AH fluxes were taken into account (Figure 12i-l). This is ascribed to the strengthened urban breeze circulations caused by the AH fluxes, which is conducive to the transmission of momentum from the upper layer to the surface. With regard to surface O_3 concentration, it increased by ~4 μg m^{-3} in the simulation with adding AH. In particular, the increases in T_2, PBLH, WS_{10} and O_3 seemed to be clearer after sunset as the solar shortwave radiation disappeared.

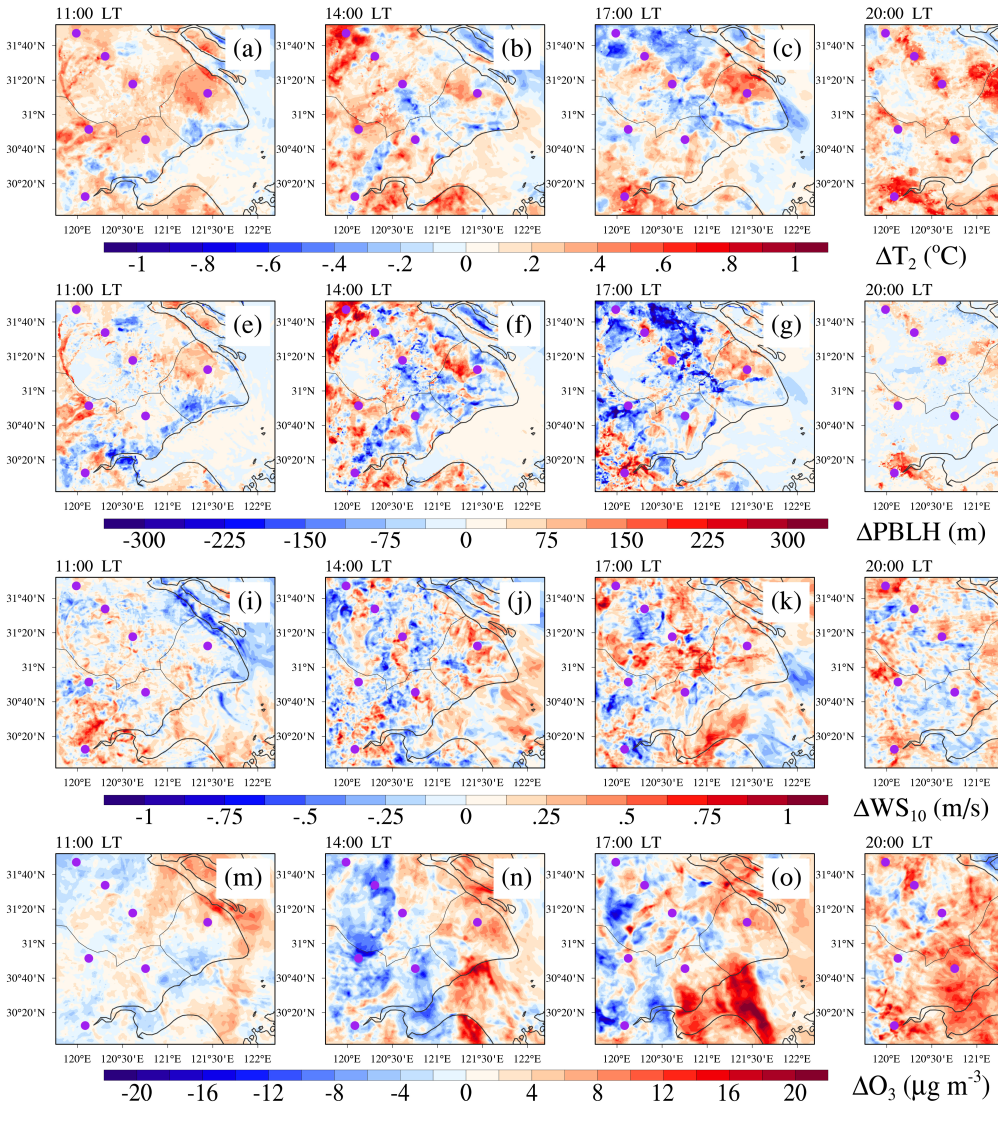

Figure 12. Same as Figure 10, but for the differences between MODIS_AH and MODIS_noAH (MODIS_AH – MODIS_noAH).

3.5.2 Vertical changes

The phenomenon that cities are almost always warmer than their surroundings is widely known as the urban heat island (UHI), and the difference between the urban and the rural surface energy balance can further induce the urban heat island circulation (UHIC). It is clearly seen that an enhanced UHIC driven by AH appeared in the megacity Shanghai around 14:00 LT (Figure 13b). This circulation extended horizontally 20-30 km from the city center to the urban edge, and vertically to ~2 km from the ground to the top of the urban boundary layer. In this case, there was a small increase (4~6 μg m^{-3}) in surface O_3. However, for the lakeside cities, the enhanced UHIC was not perceptible. And the O_3 concentration in urban areas was reduced on average, with a maximum of 16 μg m^{-3} in Wuxi around 14:00 LT (Figure 13e). The decrease in O_3 may be related to the increased wind (Figure 12i-k), which was beneficial to the diffusion and dilution of O_3. Furthermore, AH has a limited effect on the sea and lake breeze as it cannot affect any branch of the two as significantly as the urban expansion.

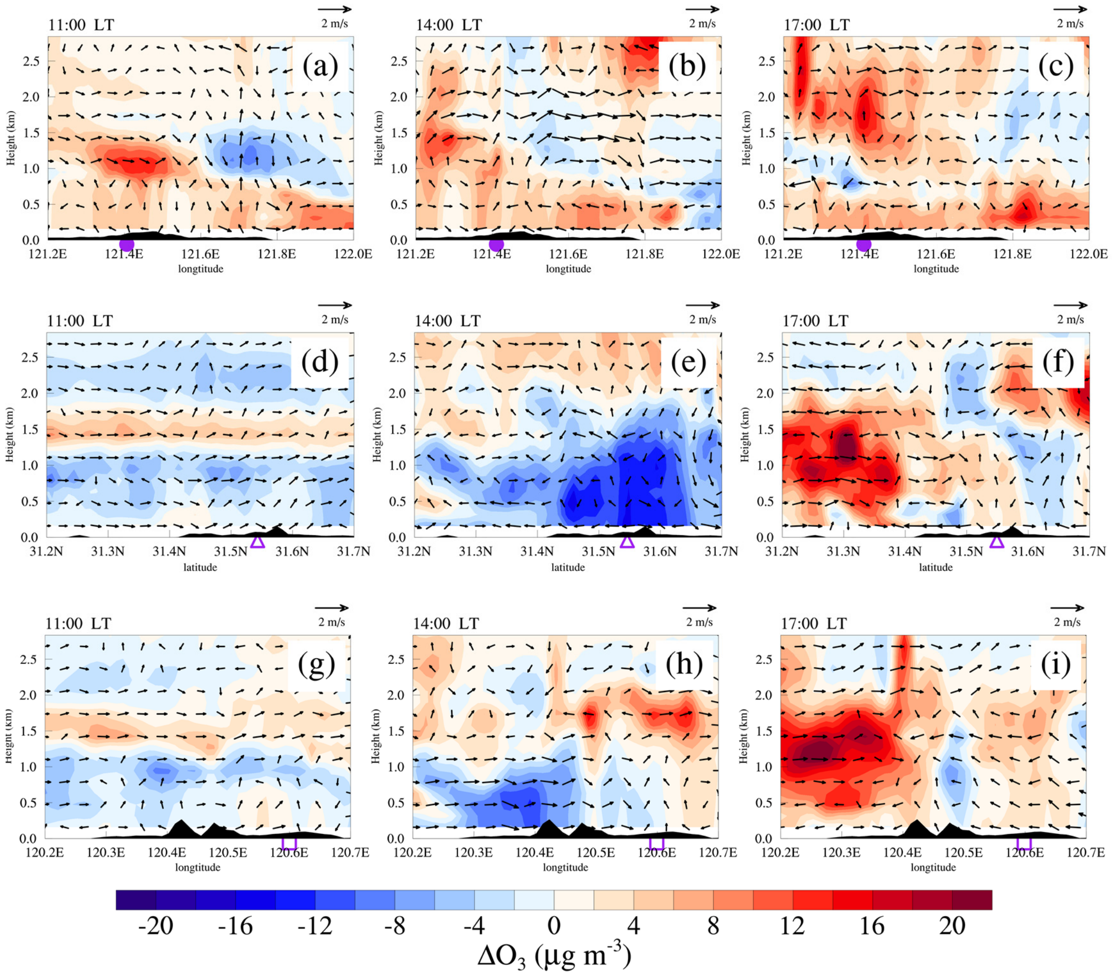

Figure 13. Same as Figure 9, but for the differences between MODIS_AH and MODIS_noAH (MODIS_AH – MODIS_noAH).

3.5.3 The mechanism of anthropogenic heat modulating O_3

AH and land use play different roles in meteorology and O_3. AH allows the atmosphere to reserve more energy via the additional sensible heat fluxes, which increases T_2 by ~0.2 °C. Higher temperature induces stronger upward air movement to the development of the convective boundary layer, rising the PBLH by ~75 m. In the convective boundary layer, the atmosphere is associated with turbulent motions, and is unstable. Together with the enhanced urban breeze caused by AH, WS_{10} increases by 0.3 m s^{-1}. These findings are comparable to the values estimated in other cities all around the world, such as Philadelphia in the United States (Fan and Sailor, 2005), Winnipeg in Canada (Ferguson and Woodbury, 2007) and Berlin in German (Menberg et al., 2013). These changes in meteorological factors eventually lead to an increase in surface O_3 by ~4 μg m^{-3}. It is noteworthy that the effects of AH are usually clearer at night in urban areas. In addition, though AH plays an important role in urban breeze circulations, it may not be powerful enough to affect the local circulations such as the sea and the lake breezes.

4 Summary and conclusions

Land use change via urban expansion and the increase of AH are important manifestations of urbanization. They can alter the regional meteorology, and thereby affect O_3 concentrations in and around cities. In this study, the YRD region, a highly urbanized coastal area with sever O_3 pollution, is selected to discuss this issue. Firstly, the basic characteristics of O_3 pollution in the YRD are investigated based on the surface observations. Secondly, a representative case is selected to further study using WRF-Chem model, and the model performance is evaluated by comparing with the observations. Finally, the response of O_3 to changes in meteorology caused by urban expansion and AH are discussed via the model inter-comparisons. The main findings are listed as below:

(1) Regional O_3 pollution occurs frequently in the YRD (~26 times per year). These O_3 pollution episodes mainly occur in calm conditions characterized by high temperature (over 20 °C), low relative humidity (less than 80%), light wind (less than 3 m s^{-1}) and shallow cloud cover (less than 5 okta). In this case, the sea and lake breezes tend to develop and have an important impact on the distribution of O_3 in this region.

(2) By updating the land use data from USGS to MODIS, we find an increase in T_2 by maximum 3 °C, an increase in PBLH by maximum 500 m and a decrease in WS_{10} by maximum 1.5 m s^{-1} in the YRD. The higher temperature and PBLH elevate surface O_3 concentration by maximum 20 μg m^{-3} via the stronger photochemical reactions and vertical mixing processes. These changes are mainly attributed to urban expansion associated with urbanization. Furthermore, the sea breeze is enhanced due to the expansion of coastal cities. Nevertheless, further progression inland of the sea breeze in the afternoon can be stalled on account of the rough urban surface, reducing the transmission of O_3 from the coast to the land. The expansion of lakeside cities extends the lifetime of the lake breeze from noon to afternoon. Since the lake breeze can accelerate the vertical mixing of O_3 in the boundary layer, the surface O_3 in lakeside cities can increase by even 30 μg m^{-3}.

(3) When the AH fluxes are taken into account, T_2, PBLH, WS_{10} and O_3 will increase by about 0.2 °C, 75 m, 0.3 m s^{-1} and 4 μg m^{-3} in and around cities. These changes are relatively small

compared to urban expansion, and mainly appear around the cities where the AH fluxes are usually large. In addition, unlike the urban expansion, AH may have a quite limited impact on the sea and the lake breezes. But the urban breeze circulations are found to be sensitive to AH inputs.

Studying the impacts of land use and AH forced by human activities on urban environment is fundamental in improving the urban air quality. Although this study only focuses on the YRD region, most of the results can be supported by previous studies that conducted in other region around the world. As more and more city clusters composed of large and medium-sized cities are being built. This work can provide valuable insight into the formation of O_3 pollution in those rapidly developing regions with unique geographical features.

Data Availability Statement.

Air quality monitoring data were acquired from a mirror of data from the official NEMC real-time publishing platform (https://quotsoft.net/air/). Meteorological data were issued by the NCDC (ftp://ftp.ncdc.noaa.gov/pub/data/noaa/isd-lite/). The FNL meteorological data were acquired from NCEP (https://doi.org/10.5065/D6M043C6/). These data can be downloaded for free as long as you agree to the official instructions.

Author contributions.

CZ and MX had the original ideas, designed the research, collected the data and prepared the original draft. CZ did the numerical simulations and carried out the data analysis. MX acquired financial support for the project leading to this publication.

Acknowledgements.

This work was supported by the National Key Research and Development Program of China (2018YFC0213502, 2018YFC1506404). We are grateful to MEPC for the air quality monitoring data, to NCDC for the meteorological data, to NCEP for global final analysis fields and to Tsinghua University for the MEIC inventories. The numerical calculations have been done on the Blade cluster system in the High Performance Computing and Massive Data Center (HPC&MDC) of School of Atmospheric Sciences, Nanjing University. We also thank the constructive comments and suggestions from the anonymous reviewers.

References

Abdi-Oskouei, M., Carmichael, G., Christiansen, M., Ferrada, G., Roozitalab, B., Sobhani, N., Wade, K., Czarnetzki, A., Pierce, R. B., Wagner, T., and Stanier, C.: Sensitivity of Meteorological Skill to Selection of WRF-Chem Physical Parameterizations and Impact on Ozone Prediction During the Lake Michigan Ozone Study (LMOS), J Geophys Res-Atmos, 125, 2020.

Bergin, M. S., West, J. J., Keating, T. J., and Russell, A. G.: Regional atmospheric pollution and transboundary air quality management, Annu. Rev. Environ. Resour., 30, 1-37, 10.1146/annurev.energy.30.050504.144138, 2005.

Blaylock, B. K., Horel, J. D., and Crosman, E. T.: Impact of Lake Breezes on Summer Ozone Concentrations in the Salt Lake Valley, Journal of Applied Meteorology and Climatology, 56, 353-370, 2017.

Buchholz, S., Junk, J., Krein, A., Heinemann, G., and Hoffmann, L.: Air pollution characteristics associated with mesoscale atmospheric patterns in northwest continental Europe, Atmospheric Environment, 44, 5183-5190, 10.1016/j.atmosenv.2010.08.053, 2010.

Chameides, W., and Walker, J. C. G.: A photochemical theory of tropospheric ozone, Journal of Geophysical Research, 78, 8751-8760, 10.1029/JC078i036p08751, 1973.

Chen, F., and Dudhia, J.: Coupling an advanced land surface-hydrology model with the Penn State-NCAR MM5 modeling system. Part II: Preliminary model validation, Monthly Weather Review, 129, 587-604, 2001.

Chen, S. H., and Sun, W. Y.: A one-dimensional time dependent cloud model, J Meteorol Soc Jpn, 80, 99-118, 2002.

Crosman, E. T., and Horel, J. D.: Sea and Lake Breezes: A Review of Numerical Studies, Boundary-Layer Meteorology, 137, 1-29, 10.1007/s10546-010-9517-9, 2010.

Ding, A., Wang, T., Zhao, M., Wang, T., and Li, Z.: Simulation of sea-land breezes and a discussion of their implications on the transport of air pollution during a multi-day ozone episode in the Pearl River Delta of China, Atmospheric Environment, 38, 6737-6750, 10.1016/j.atmosenv.2004.09.017, 2004.

Fan, H. L., and Sailor, D. J.: Modeling the impacts of anthropogenic heating on the urban climate of Philadelphia: a comparison of implementations in two PBL schemes, Atmospheric

Environment, 39, 73-84, 2005.

Fast, J. D., Gustafson, W. I., Easter, R. C., Zaveri, R. A., Barnard, J. C., Chapman, E. G., Grell, G. A., and Peckham, S. E.: Evolution of ozone, particulates, and aerosol direct radiative forcing in the vicinity of Houston using a fully coupled meteorology-chemistry-aerosol model, J Geophys Res-Atmos, 111, 2006.

Ferguson, G., and Woodbury, A. D.: Urban heat island in the subsurface, Geophysical Research Letters, 34, 2007.

Flanner, M. G.: Integrating anthropogenic heat flux with global climate models, Geophysical Research Letters, 36, n/a-n/a, 10.1029/2008gl036465, 2009.

Freitas, E. D., Rozoff, C. M., Cotton, W. R., and Dias, P. L. S.: Interactions of an urban heat island and sea-breeze circulations during winter over the metropolitan area of Sao Paulo, Brazil, Boundary-Layer Meteorology, 122, 43-65, 2007.

Friedl, M. A., Sulla-Menashe, D., Tan, B., Schneider, A., Ramankutty, N., Sibley, A., and Huang, X.: MODIS Collection 5 global land cover: Algorithm refinements and characterization of new datasets, Remote Sensing of Environment, 114, 168-182, 10.1016/j.rse.2009.08.016, 2010.

Fu, Y. and Liao, H.: Impacts of land use and land cover changes on biogenic emissions of volatile organic compounds in China from the late 1980s to the mid-2000s: implications for tropospheric ozone and secondary organic aerosol, Tellus B: Chemical and Physical Meteorology, 66, 10.3402/tellusb.v66.24987, 2014.

Gao, D., Xie, M., Chen, X., Wang, T. J., Liu, J., Xu, Q., Mu, X. Y., Chen, F., Li, S., Zhuang, B. L., Li, M. M., Zhao, M., and Ren, J. Y.: Systematic classification of circulation patterns and integrated analysis of their effects on different ozone pollution levels in the Yangtze River Delta Region, China, Atmospheric Environment, 242, 2020.

Gong, P., Liu, H., Zhang, M., Li, C., Wang, J., Huang, H., Clinton, N., Ji, L., Li, W., Bai, Y., Chen, B., Xu, B., Zhu, Z., Yuan, C., Ping Suen, H., Guo, J., Xu, N., Li, W., Zhao, Y., Yang, J., Yu, C., Wang, X., Fu, H., Yu, L., Dronova, I., Hui, F., Cheng, X., Shi, X., Xiao, F., Liu, Q., and Song, L.: Stable classification with limited sample: transferring a 30-m resolution sample set collected in 2015 to mapping 10-m resolution global land cover in 2017, Science Bulletin, 64, 370-373, 10.1016/j.scib.2019.03.002, 2019.

Grell, G. A., and Dévényi, D.: A generalized approach to parameterizing convection combining ensemble and data assimilation techniques, Geophysical Research Letters, 29, 38-31-38-34, 10.1029/2002gl015311, 2002.

Grell, G. A., Peckham, S. E., Schmitz, R., McKeen, S. A., Frost, G., Skamarock, W. C., and Eder, B.: Fully coupled "online" chemistry within the WRF model, Atmospheric Environment, 39, 6957-6975, 10.1016/j.atmosenv.2005.04.027, 2005.

Guenther, A., Karl, T., Harley, P., Wiedinmyer, C., Palmer, P. I., and Geron, C.: Estimates of global terrestrial isoprene emissions using MEGAN (Model of Emissions of Gases and Aerosols from Nature), Atmospheric Chemistry and Physics, 6, 3181-3210, 2006.

Hong, S. Y., Noh, Y., and Dudhia, J.: A new vertical diffusion package with an explicit treatment of entrainment processes, Monthly Weather Review, 134, 2318-2341, 2006.

Hu, J., Li, Y., Zhao, T., Liu, J., Hu, X.-M., Liu, D., Jiang, Y., Xu, J., and Chang, L.: An important mechanism of regional O₃ transport for summer smog over the Yangtze River Delta in eastern China, Atmospheric Chemistry and Physics, 18, 16239-16251, 10.5194/acp-18-16239-2018, 2018.

Jacob, D. J., and Winner, D. A.: Effect of climate change on air quality, Atmospheric Environment, 43, 51-63, 10.1016/j.atmosenv.2008.09.051, 2009.

Jerrett, M., Burnett, R. T., Pope, C. A., Ito, K., Thurston, G., Krewski, D., Shi, Y. L., Calle, E., and Thun, M.: Long-Term Ozone Exposure and Mortality., New Engl J Med, 360, 1085-1095, 2009.

Jiang, X., Wiedinmyer, C., Chen, F., Yang, Z.-L., and Lo, J. C.-F.: Predicted impacts of climate and land use change on surface ozone in the Houston, Texas, area, Journal of Geophysical Research, 113, 10.1029/2008jd009820, 2008.

Jimenez, P. A., and Dudhia, J.: Improving the Representation of Resolved and Unresolved Topographic Effects on Surface Wind in the WRF Model, Journal of Applied Meteorology and Climatology, 51, 300-316, 2012.

Kim, H.-J., and Wang, B.: Sensitivity of the WRF model simulation of the East Asian summer monsoon in 1993 to shortwave radiation schemes and ozone absorption, Asia-Pacific Journal of Atmospheric Sciences, 47, 167-180, 10.1007/s13143-011-0006-y, 2011.

Lennartson, G. J., and Schwartz, M. D.: The lake breeze-ground-level ozone connection in eastern Wisconsin: A climatological perspective, International Journal of Climatology, 22, 1347-1364, 2002.

Li, K., Jacob, D. J., Shen, L., Lu, X., De Smedt, I., and Liao, H.: Increases in surface ozone pollution in China from 2013 to 2019: anthropogenic and meteorological influences, Atmospheric Chemistry and Physics, 20, 11423-11433, 10.5194/acp-20-11423-2020, 2020.

Li, M., Song, Y., Huang, X., Li, J., Mao, Y., Zhu, T., Cai, X., and Liu, B.: Improving mesoscale modeling using satellite-derived land surface parameters in the Pearl River Delta region, China, Journal of Geophysical Research: Atmospheres, 119, 6325-6346, 10.1002/2014jd021871, 2014.

Li, M., Wang, T., Xie, M., Zhuang, B., Li, S., Han, Y., Song, Y., and Cheng, N.: Improved meteorology and ozone air quality simulations using MODIS land surface parameters in the Yangtze River Delta urban cluster, China, Journal of Geophysical Research: Atmospheres, 122, 3116-3140, 10.1002/2016jd026182, 2017.

Li, Y., Zhang, J., Sailor, D. J., and Ban-Weiss, G. A.: Effects of urbanization on regional meteorology and air quality in Southern California, Atmospheric Chemistry and Physics, 19, 4439-4457, 10.5194/acp-19-4439-2019, 2019.

Liao, Z., Gao, M., Sun, J., and Fan, S.: The impact of synoptic circulation on air quality and pollution-related human health in the Yangtze River Delta region, Sci Total Environ, 607-608, 838-846, 10.1016/j.scitotenv.2017.07.031, 2017.

Lin, C. H., Lai, C. H., Wu, Y. L., Lin, P. H., and Lai, H. C.: Impact of sea breeze air masses laden with ozone on inland surface ozone concentrations: A case study of the northern coast of Taiwan, J Geophys Res-Atmos, 112, 2007.

Liu, M., and Tian, H.: China's land cover and land use change from 1700 to 2005: Estimations from high-resolution satellite data and historical archives, Global Biogeochemical Cycles, 24, n/a-n/a, 10.1029/2009gb003687, 2010.

Loveland, T. R., Reed, B. C., Brown, J. F., Ohlen, D. O., Zhu, Z., Yang, L., and Merchant, J. W.: Development of a global land cover characteristics database and IGBP DISCover from 1 km AVHRR data, International Journal of Remote Sensing, 21, 1303-1330, 10.1080/014311600210191, 2000.

Lu, X., Hong, J., Zhang, L., Cooper, O. R., Schultz, M. G., Xu, X., Wang, T., Gao, M., Zhao, Y., and Zhang, Y.: Severe Surface Ozone Pollution in China: A Global Perspective, Environmental Science & Technology Letters, 5, 487-494, 10.1021/acs.estlett.8b00366, 2018.

Mavrakou, T., Philippopoulos, K., and Deligiorgi, D.: The impact of sea breeze under different synoptic patterns on air pollution within Athens basin, Science of the Total Environment, 433, 31-43, 2012.

Menberg, K., Bayer, P., Zosseder, K., Rumohr, S., and Blum, P.: Subsurface urban heat islands in German cities, Sci Total Environ, 442, 123-133, 10.1016/j.scitotenv.2012.10.043, 2013.

Miao, Y., Hu, X.-M., Liu, S., Qian, T., Xue, M., Zheng, Y., and Wang, S.: Seasonal variation of local atmospheric circulations and boundary layer structure in the Beijing-Tianjin-Hebei region and implications for air quality, Journal of Advances in Modeling Earth Systems, 7, 1602-1626, 10.1002/2015ms000522, 2015.

Mills, G., Hayes, F., Simpson, D., Emberson, L., Norris, D., Harmens, H., and Buker, P.: Evidence of widespread effects of ozone on crops and (semi-)natural vegetation in Europe (1990-2006) in relation to AOT40-and flux-based risk maps, Glob. Change Biol., 17, 592-613, 10.1111/j.1365-2486.2010.02217.x, 2011.

Mlawer, E. J., Taubman, S. J., Brown, P. D., Iacono, M. J., and Clough, S. A.: Radiative transfer for inhomogeneous atmospheres: RRTM, a validated correlated-k model for the longwave, Journal of Geophysical Research: Atmospheres, 102, 16663-16682, 10.1029/97jd00237, 1997.

Oke, T. R.; Mills, G.; Christen, A.; Voogt, J. A. Urban Climates; Cambridge University Press: Cambridge, 2017.

Park, R. J., Hong, S. K., Kwon, H. A., Kim, S., Guenther, A., Woo, J. H., and Loughner, C. P.: An evaluation of ozone dry deposition simulations in East Asia, Atmospheric Chemistry and Physics, 14, 7929-7940, 10.5194/acp-14-7929-2014, 2014.

Ryu, Y.-H., Baik, J.-J., and Lee, S.-H.: Effects of anthropogenic heat on ozone air quality in a megacity, Atmospheric Environment, 80, 20-30, 10.1016/j.atmosenv.2013.07.053, 2013.

Sailor, D. J.: A review of methods for estimating anthropogenic heat and moisture emissions in the urban environment, International Journal of Climatology, 31, 189-199, 10.1002/joc.2106, 2011.

Sati, A. P., and Mohan, M.: The impact of urbanization during half a century on surface meteorology based on WRF model simulations over National Capital Region, India, Theoretical and Applied Climatology, 134, 309-323, 2017.

Schell, B., Ackermann, I. J., Hass, H., Binkowski, F. S., and Ebel, A.: Modeling the formation of secondary organic aerosol within a comprehensive air quality model system, J Geophys Res-

Atmos, 106, 28275-28293, 2001.

Sills, D. M. L., Brook, J. R., Levy, I., Makar, P. A., Zhang, J., and Taylor, P. A.: Lake breezes in the southern Great Lakes region and their influence during BAQS-Met 2007, Atmospheric Chemistry and Physics, 11, 7955-7973, 10.5194/acp-11-7955-2011, 2011.

Stockwell, W. R., Middleton, P., Chang, J. S., and Tang, X. Y.: The 2nd Generation Regional Acid Deposition Model Chemical Mechanism for Regional Air-Quality Modeling, J Geophys Res-Atmos, 95, 16343-16367, 1990.

Wang, T., Xue, L., Brimblecombe, P., Lam, Y. F., Li, L., and Zhang, L.: Ozone pollution in China: A review of concentrations, meteorological influences, chemical precursors, and effects, Sci Total Environ, 575, 1582-1596, 10.1016/j.scitotenv.2016.10.081, 2017.

Wang, X., Chen, F., Wu, Z., Zhang, M., Tewari, M., Guenther, A., and Wiedinmyer, C.: Impacts of weather conditions modified by urban expansion on surface ozone: Comparison between the Pearl River Delta and Yangtze River Delta regions, Advances in Atmospheric Sciences, 26, 962-972, 10.1007/s00376-009-8001-2, 2009.

Wang, Y., Gao, W., Wang, S., Song, T., Gong, Z., Ji, D., Wang, L., Liu, Z., Tang, G., Huo, Y., Tian, S., Li, J., Li, M., Yang, Y., Chu, B., Petäjä, T., Kerminen, V.-M., He, H., Hao, J., Kulmala, M., Wang, Y., and Zhang, Y.: Contrasting trends of $PM_{2.5}$ and surface-ozone concentrations in China from 2013 to 2017, National Science Review, 7, 1331-1339, 10.1093/nsr/nwaa032, 2020.

Wentworth, G. R., Murphy, J. G., and Sills, D. M. L.: Impact of lake breezes on ozone and nitrogen oxides in the Greater Toronto Area, Atmospheric Environment, 109, 52-60, 10.1016/j.atmosenv.2015.03.002, 2015.

Worden, H. M., Bowman, K. W., Worden, J. R., Eldering, A., and Beer, R.: Satellite measurements of the clear-sky greenhouse effect from tropospheric ozone, Nature Geoscience, 1, 305-308, 2008.

Xie, M., Liao, J., Wang, T., Zhu, K., Zhuang, B., Han, Y., Li, M., and Li, S.: Modeling of the anthropogenic heat flux and its effect on regional meteorology and air quality over the Yangtze River Delta region, China, Atmospheric Chemistry and Physics, 16, 6071-6089, 10.5194/acp-16-6071-2016, 2016a.

Xie, M., Shu, L., Wang, T.-j., Liu, Q., Gao, D., Li, S., Zhuang, B.-l., Han, Y., Li, M.-m., and Chen, P.-l.: Natural emissions under future climate condition and their effects on surface ozone in the

Yangtze River Delta region, China, Atmospheric Environment, 150, 162-180, 10.1016/j.atmosenv.2016.11.053, 2017.

Xie, M., Zhu, K., Wang, T., Feng, W., Gao, D., Li, M., Li, S., Zhuang, B., Han, Y., Chen, P., and Liao, J.: Changes in regional meteorology induced by anthropogenic heat and their impacts on air quality in South China, Atmospheric Chemistry and Physics, 16, 15011-15031, 10.5194/acp-16-15011-2016, 2016b.

Xie, M., Zhu, K., Wang, T, Yang, H., Zhuang, B., Li, S., Li, M., Zhu, X., and Ouyang, Y.: Application of photochemical indicators to evaluate ozone nonlinear chemistry and pollution control countermeasure in China, Atmospheric Environment, 99, 466-473, 10.1016/j.atmosenv.2014.10.013, 2014.

You, C., Fung, J. C. H., and Tse, W. P.: Response of the Sea Breeze to Urbanization in the Pearl River Delta Region, Journal of Applied Meteorology and Climatology, 58, 1449-1463, 2019.

Young, P. J., Archibald, A. T., Bowman, K. W., Lamarque, J. F., Naik, V., Stevenson, D. S., Tilmes, S., Voulgarakis, A., Wild, O., Bergmann, D., Cameron-Smith, P., Cionni, I., Collins, W. J., Dalsøren, S. B., Doherty, R. M., Eyring, V., Faluvegi, G., Horowitz, L. W., Josse, B., Lee, Y. H., MacKenzie, I. A., Nagashima, T., Plummer, D. A., Righi, M., Rumbold, S. T., Skeie, R. B., Shindell, D. T., Strode, S. A., Sudo, K., Szopa, S., and Zeng, G.: Pre-industrial to end 21st century projections of tropospheric ozone from the Atmospheric Chemistry and Climate Model Intercomparison Project (ACCMIP), Atmospheric Chemistry and Physics, 13, 2063-2090, 10.5194/acp-13-2063-2013, 2013.

Yu, M., Carmichael, G. R., Zhu, T., and Cheng, Y.: Sensitivity of predicted pollutant levels to urbanization in China, Atmospheric Environment, 60, 544-554, 10.1016/j.atmosenv.2012.06.075, 2012.

Zhan, C., Xie, M., Huang, C., Liu, J., Wang, T., Xu, M., Ma, C., Yu, J., Jiao, Y., Li, M., Li, S., Zhuang, B., Zhao, M., and Nie, D.: Ozone affected by a succession of four landfall typhoons in the Yangtze River Delta, China: major processes and health impacts, Atmospheric Chemistry and Physics, 20, 13781-13799, 10.5194/acp-20-13781-2020, 2020.

Zhan, C., Xie, M., Liu, J., Wang, T., Xu, M., Chen, B., Li, S., Zhuang, B., and Li, M.: Surface Ozone in the Yangtze River Delta, China: A Synthesis of Basic Features, Meteorological Driving Factors, and Health Impacts, Journal of Geophysical Research: Atmospheres, 126, 10.1029/2020jd033600, 2021.

Zhan, C.-c., Xie, M., Fang, D.-x., Wang, T.-j., Wu, Z., Lu, H., Li, M.-m., Chen, P.-l., Zhuang, B.-l., Li, S., Zhang, Z.-q., Gao, D., Ren, J.-y., and Zhao, M.: Synoptic weather patterns and their impacts on regional particle pollution in the city cluster of the Sichuan Basin, China, Atmospheric Environment, 208, 34-47, 10.1016/j.atmosenv.2019.03.033, 2019.

Zhang, N., Zhu, L., and Zhu, Y.: Urban heat island and boundary layer structures under hot weather synoptic conditions: A case study of Suzhou City, China, Advances in Atmospheric Sciences, 28, 855-865, 10.1007/s00376-010-0040-1, 2011.

Zhang, H., Wang, Y., Hu, J., Ying, Q., and Hu, X. M.: Relationships between meteorological parameters and criteria air pollutants in three megacities in China, Environ Res, 140, 242-254, 10.1016/j.envres.2015.04.004, 2015.

Zhu, B., Kang, H., Zhu, T., Su, J., Hou, X., and Gao, J.: Impact of Shanghai urban land surface forcing on downstream city ozone chemistry, Journal of Geophysical Research: Atmospheres, 120, 4340-4351, 10.1002/2014jd022859, 2015.